Single-Molecule Ultrafast Fluorescence-Detected Pump–Probe Microscopy

Daniel Fersch[1§], Pavel Malý[1,2§], Jessica Rühe[3], Victor Lisinetskii[1], Matthias Hensen[1], Frank Würthner[3,4], and Tobias Brixner[1,4]*

[1]Universität Würzburg, Institut für Physikalische und Theoretische Chemie, Am Hubland, 97074 Würzburg, Germany

[2]Charles University, Faculty of Mathematics and Physics, Ke Karlovu 5, 121 16 Prague, Czech Republic

[3]Universität Würzburg, Institut für Organische Chemie, Am Hubland, 97074 Würzburg, Germany

[4]Universität Würzburg, Center for Nanosystems Chemistry (CNC), Theodor-Boveri-Weg, 97074 Würzburg, Germany

AUTHOR INFORMATION

Corresponding Author

*brixner@uni-wuerzburg.de

§D.F. and P.M. contributed equally to this paper.

ABSTRACT. We introduce fluorescence-detected pump–probe microscopy by combining a wavelength-tunable ultrafast laser with a confocal scanning fluorescence microscope, enabling access to the femtosecond time scale on the micrometer spatial scale. In addition, we obtain spectral information from Fourier transformation over excitation pulse-pair time delays. We demonstrate this new approach on a model system of a terrylene bisimide (TBI) dye embedded in a PMMA matrix and acquire the linear excitation spectrum as well as time-dependent pump–probe spectra simultaneously. We then push the technique towards single TBI molecules and analyze the statistical distribution of their excitation spectra. Furthermore, we demonstrate the ultrafast transient evolution of several individual molecules, highlighting their different behavior in contrast to the ensemble due to their individual local environment. By correlating the linear and nonlinear spectra, we assess the effect of the molecular environment on the excited-state energy.

TOC GRAPHICS

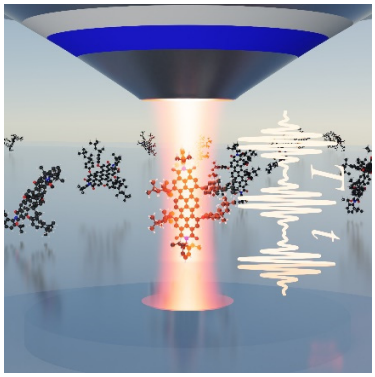

KEYWORDS. Excited states, Fluorescence, Fluorescence detection, Ultrafast spectroscopy, Electronic spectroscopy, Single-Molecule Microscopy, Wave-packet dynamics

Beginning with the pioneering experiments by Moerner and Orrit,[1–5] methods and applications for the imaging and spectroscopy of individual molecules have found widespread application in the life and material sciences. The quantum nature of single-molecule optical transitions can provide access to quantum light[6,7], and the associated stochastic photo-switching between bright and dark states as well as their narrow spectral linewidths in contrast to the ensemble lay the foundation for super-resolution microscopy methods that have led to high-precision imaging.[8–15]

Most single-molecule techniques rely on the fact that after initial excitation with light, individual dye molecules re-emit a single photon of light with a probability determined by the quantum yield of the molecule. The properties of the excited states are not only specific to each type of molecule but can also significantly vary depending on the molecule's local environment.[16] For this reason, the spectra and kinetics of individual molecules can be used as highly local probes and have been shown to be sensitive to the presence of functionalized nanostructures[17–22] and the morphology of macromolecular material systems.[23–27] They have further found broad application in biomolecule tagging and for studying dynamical processes in biological systems.[8,28–31] The excited-state lifetime of a typical molecule is usually in the range of hundreds of picoseconds or longer, and as such can be measured using time-correlated single-photon counting (TCSPC).

However, many intra- and intermolecular processes take place on femtosecond timescales, which cannot be captured by TCSPC with its relatively low temporal resolution. This is where ultrafast nonlinear techniques are commonly used, such as ultrafast pump–probe (PP) spectroscopy, also known as transient absorption.[32] There, transient molecular spectra are obtained by adjusting the time delay between two individual ultrashort laser pulses, a pump and a probe, yielding ultrafast temporal resolution that is in principle only limited by the pulse length. Extending this nonlinear spectroscopy technique to the single-molecule regime is very difficult as these experiments are

commonly associated with high pump pulse energies to achieve a satisfactory signal-to-noise ratio, which is often not compatible with the limited photo- and thermal stability of a single molecule. In addition, the change in probe intensity caused by an individual molecule will always be very small, so considerable effort has to be invested to isolate the desired signal from the comparatively large background of the unaffected probe laser beam,[33,34] which is why a majority of single-molecule experiments rely on the detection of background-free fluorescence instead.[35]

While ultrafast spectroscopy of individual quantum objects such as, e.g., single quantum dots[36–39] or carbon nanotubes,[40] has been performed, capturing the ultrafast dynamics of single molecules remains very challenging due to their fragile nature in comparison to solid-state quantum emitters. Recent work in this direction includes femtosecond orbital imaging by THz scanning tunneling microscopy,[41] investigation of ultrafast fluorescence lifetimes in single dye molecules coupled to plasmonic nanostructures,[42] ultrafast energetic relaxation and energy transfer in single photosynthetic complexes,[43–46] and observation of ultrafast dynamics in single molecules.[47,48] These experiments, with one exception,[41] are based on measuring the fluorescence yield as a function of the time delay between pump and probe pulse. They did not access spectral information as in a conventional transient absorption experiment, which makes it difficult to disentangle the various relaxation pathways of the excited molecule by the corresponding signal contributions that can lead to a single pump–probe transient. Liebel et al. demonstrated spectral resolution in a two-color stimulated emission experiment, where spectral information was obtained by modulating the probe pulse into a pulse pair by means of amplitude masks generated by a pulse shaper.[49] However, the necessity for two spectrally separate colors and the required extensive discussion of the shaping process to generate the probe pulse pair makes the experiment not as straightforward to apply in comparison to conventional pump–probe spectroscopy.

In the present work, we demonstrate pump–probe spectroscopy, including spectral resolution, down to the single-molecule limit. We generate time delays between spectrally identical laser pulses using mechanical delay lines. This avoids complex geometries and makes the experimental implementation straightforward. We combine spectrally resolved, fluorescence-detected pump–probe (F-PP) spectroscopy, recently developed by some of us,[50] with confocal microscopy to measure the spectrally resolved ultrafast dynamics of single molecules and use the simultaneous acquisition of linear and nonlinear spectra to investigate the effect of the local environment on the molecular transition frequencies.

The principle of F-PP microscopy is sketched in Figure 1a, assuming an electronic two-level system with vibrational sublevels as a convenient model for a dye molecule. First, an ultrashort laser pulse (blue, subsequently referred to as the pump pulse) is used to excite the system from its initial ground state $|g\rangle$ to an electronically (and potentially vibrationally) excited state $|e\rangle$. Then, the system evolves for a specified waiting time T, during which numerous processes such as wave-packet dynamics, energy transfer or vibrational relaxation can take place. Then the system is probed with a pair of pulses (orange), where the first probe pulse converts the population state into a coherent superposition between the ground and excited electronic states. This superposition oscillates in time with a frequency that is proportional to the energy gap of the involved superposition states and is sampled with the second probe (third in total) pulse, preparing a population state. This state then decays via spontaneous emission, which serves as the measurement signal. Temporal information is then obtained by scanning T and spectral information by scanning t and subsequent Fourier transformation.

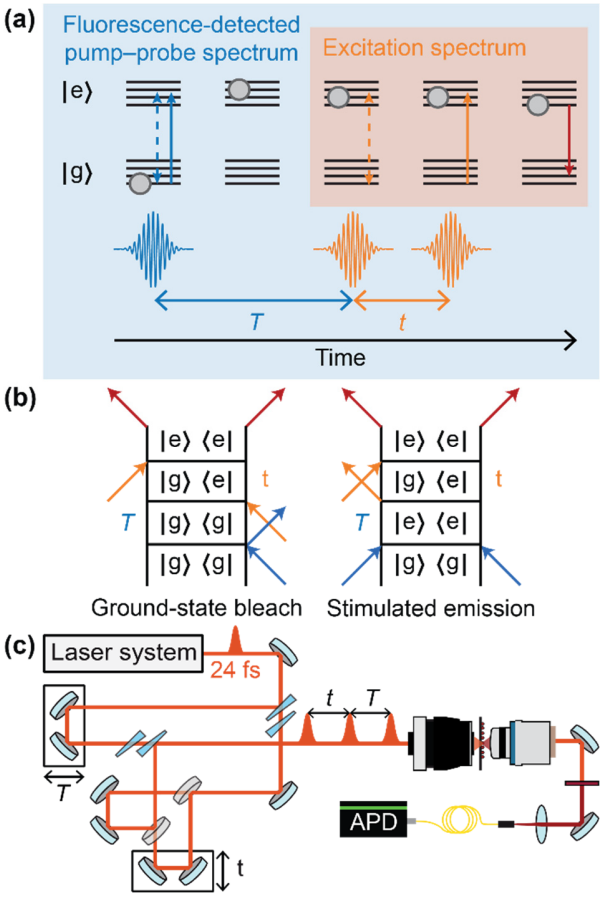

Figure 1. Principle of F-PP microscopy. (a) Schematic of the three-pulse sequence used for pumping and probing an electronic two-level system with vibrational sublevels. Colored boxes indicate the two types of spectra obtained in an F-PP measurement from scanning inter-pulse delays *T* and *t*, followed by Fourier transformation over *t*. (b) The two main signal contributions of F-PP represented as double-sided Feynman diagrams. Individual interactions with the pump and probe fields are indicated by blue and orange arrows, respectively, whereas the dark-red arrows indicate spontaneous emission. (c) Experimental setup. Ultrashort pulses are generated and split into three pulses with adjustable time delays *T* and *t* using two nested Mach–Zehnder interferometers. The sample is excited with this pulse train through a microscope objective and sample fluorescence is collected with a second objective. Fluorescence is separated from the excitation light with long-pass filters and detected by a fiber-coupled single-photon counter (avalanche photodiode, APD).

To remove any linear contributions to the spectrum, this measurement is repeated without the pump pulse for each waiting time *T* and the resulting interferogram is subtracted. As this linear

contribution is equivalent to the result of a conventional double-pulse excitation spectrum measurement,[51,52] two spectra are obtained in the measurement process – the nonlinear, fluorescence-detected PP spectrum as well as the linear excitation spectrum of the molecule, indicated as colored boxes in Figure 1a.

The measurement principle can be described in the language of double-sided Feynman diagrams (Figure 1b). In this formalism, the system is described by its density matrix, where the diagonal and off-diagonal elements denote the population of specific states and their mutual coherence, respectively. Each arrow denotes an interaction with the electric field, exciting or deexciting the system. We observe such signals in which the pump pulse interacts twice to generate a population and each probe pulse only interacts once. This gives rise to signal contributions (from fluorescence) that can be understood in the context of transient absorption spectroscopy, such as ground-state bleach and stimulated emission.

The resulting measurement signal is incoherent in nature, and there is no inherent phase-matching condition involved. This enables us to perform the experiment in a fully collinear geometry with subsequent spectral filtering of the red-shifted fluorescence, and thus the method is ideally suited for combination with fluorescence microscopy (Figure 1c). We employ two nested Mach–Zehnder interferometers to generate three compressed ultrashort pulses in the visible spectral range with individually adjustable inter-pulse time delays T and t, which are then guided into a fluorescence microscope of our own design. A reflective objective is used for exciting the sample, making the setup compatible with a wide range of excitation wavelengths and broad spectra without introducing any additional dispersion to the laser pulses. Sample fluorescence is collected with a refractive microscope objective, separated from excitation light by long-pass filters, and detected by a single-photon counting avalanche photodiode (APD) connected to a single-mode fiber,

enabling confocal detection from a diffraction-limited spot (see Methods). Microscopy images are generated by scanning the sample laterally through the laser focus.

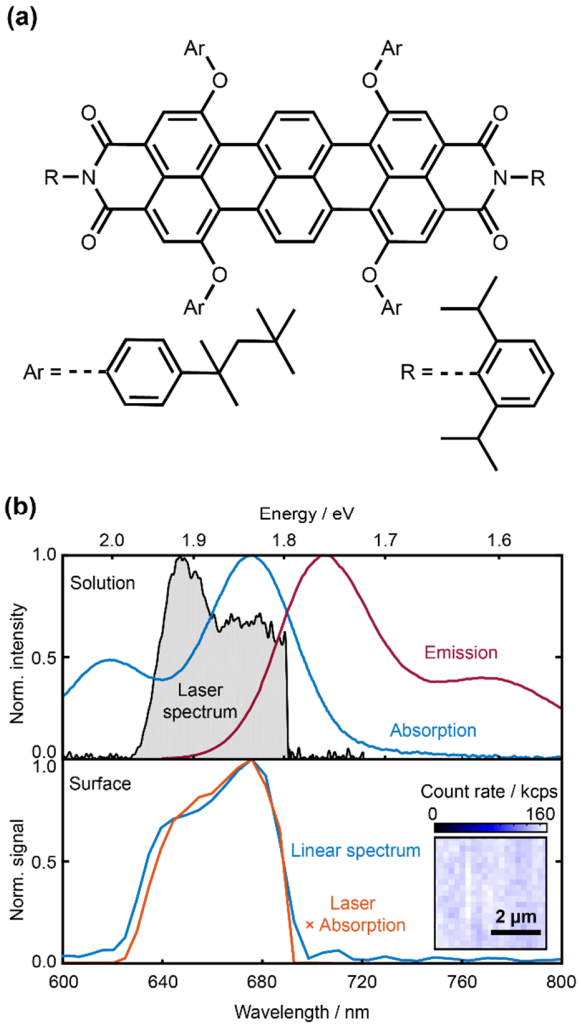

Figure 2. Molecular system as well as linear reference spectra. (a) Structural formula of the terrylene bisimide (TBI) used as a model system. (b) Top: Liquid-phase absorption (blue) and emission spectrum (dark red) of TBI in toluene with the laser spectrum used in all measurements (grey). Bottom: Linear spectrum (blue) of a spin-coated sample of TBI in PMMA matrix and the expectation from theory (red). The inset shows a spatial microscope scan of the sample that has a homogeneous appearance.

As a model system for our experiments we chose a highly stable substituted terrylene bisimide (TBI) molecule (Figure 2a).[53,54] We covered the main absorption band of the S_0-S_1 transition at

1.83 eV with our laser spectrum and detected the red-shifted molecular fluorescence (Figure 2b). The laser spectrum was blocked in the detection channel for photon energies below 1.79 eV using a long-pass filter to avoid any overlap with the fluorescence signal.

For our first experiments, we spin-coated TBI and poly(methyl methacrylate) (PMMA) to prepare an "ensemble" sample (see Methods), serving as a reference for the single-molecule study to be discussed later (see Supporting Information S3 for a discussion on the morphology of the ensemble sample). A microscope image of this homogeneous sample is shown in the inset of Figure 2b, where no heterogeneities are seen except for minor count fluctuations attributed to the lack of averaging when acquiring images. To ensure that the photon counts arise from TBI molecules on the surface, we analyze the linear spectrum obtained from a double-pulse scan as explained above. The shape of this spectrum is not only given by the molecular response but is additionally weighted by the shape of the laser spectrum, i.e., the linear spectrum retrieved by the F-PP measurement should be equivalent to the multiplication of the laser spectrum and the excitation spectrum. The excitation spectrum in turn agrees with the absorption spectrum if the fluorescence quantum yield is wavelength-independent. In Figure 2b, we compare this linear spectrum (blue) with the multiplication of the laser spectrum and the molecular absorption spectrum in toluene (red). We find a good match so that we indeed attribute the detected fluorescence photons to the TBI molecules. Further, we can also conclude that when changing the environment from PMMA to toluene, no spectral shift is observed as the linear spectra of both are in good agreement. As this linear signal is independent of the waiting time T, we use it as a monitoring signal to check if the spectrum changes over the course of the measurement, e.g., to correct for the slow photobleaching of the ensemble sample, or to check for spectral diffusion in the case of single-molecule samples.

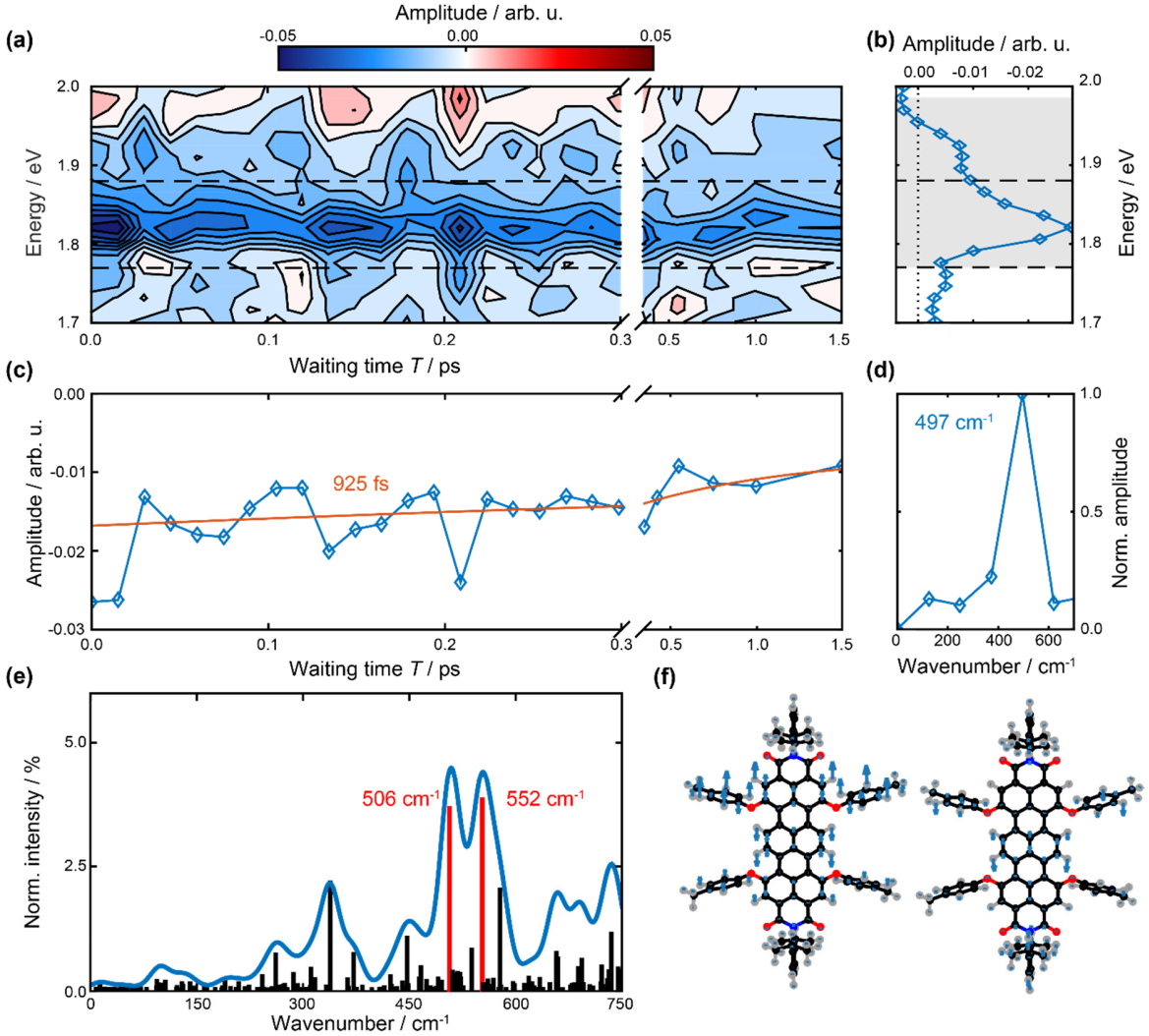

Figure 3. F-PP micro-spectroscopy of ensemble TBI. (a) Time-resolved F-PP spectrum with linear sampling up to 0.3 ps and subsequent nonlinear sampling. Spectral integration limits for the time trace are indicated with dashed lines. (b) F-PP spectrum integrated over *T*. The grey-shaded area indicates the signal window, and the dotted lines give an estimation of the noise floor, both for positive and negative signals (Supporting Information, Section S4). (c) Spectrally integrated time trace of the F-PP signal (blue), showing the negative, decaying signal as well as oscillatory behavior, and kinetic exponential fit (red) with extracted time constant. (d) Power spectrum of the linearly sampled part of fitting residuals with wavenumber of the peak. (e) Simulated IR spectrum at the B3LYP/6-31G(d) level of TBI with (1,1,3,3-tetramethylbutyl) chains replaced by methyl groups. The stick spectrum is given in black, while a spectrally line-broadened version is shown in blue. The wavenumbers of the two most prominent vibrations in the experimentally relevant spectral region are marked and given in red. (f) Sketch of the molecular vibrations indicated in red in (e).

We now analyze the time-dependent F-PP spectrum of the ensemble sample (Figure 3a). A strong negative broad signal contribution, corresponding to ground-state bleach and stimulated emission, is seen with a peak value at 1.82 eV and a full width at half maximum (FWHM) of 62 meV, corresponding to the main absorption peak of TBI at 1.83 eV. This signal contribution decays slowly with waiting time but has not yet vanished at 1.5 ps waiting time delay, which is the edge of our measurement window. For further illustration, we integrated this spectrum over the waiting time axis (Figure 3b). Except for minor baseline fluctuations, no signal is observed outside of the signal window (as given by the foot-to-foot range of the laser spectrum measured by linear autocorrelation), which is what we expect. The spectrum also provides a reference for much noisier single-molecule spectra discussed below.

To analyze the time-dependent evolution of the F-PP spectrum, we integrated the spectrum from 1.77 to 1.88 eV to obtain the associated time trace (Figure 3c), which was fitted with a kinetic function of the form

$$y(T) = a\, e^{-k_T T} + c,$$

where k_T is a mono-exponential decay rate and a and c are suitable parameters. This function was chosen because our temporal measurement window could not capture the long excited-state lifetime on the order of nanoseconds associated with TBI molecules on surfaces.[55] Instead, this long lifetime can be seen as a constant offset c in the fitting function. For the exponential decay, we obtain $k_T = 1.1$ ps^{-1}, corresponding to a time constant of 925 fs. We attribute this time constant to vibrational cooling in the first excited electronic state, manifesting as a decay of the stimulated emission that becomes red-shifted out of our probe window. Since this internal relaxation process is directly captured by the interaction with the probe pulse pair, we can follow it in the F-PP spectrum despite us measuring the incoherent fluorescence signal.

As seen in Figure 3c, a mono-exponential decay is not sufficient to capture the full dynamics of the measured data. To investigate this further, we subtracted the fit from the data and Fourier-transformed the resulting residuals from 0 to 300 fs to obtain a power spectrum (Figure 3d), in which we observe a single peak at 497 cm^{-1}. Similar values have been reported for vibronic coherences in TBI monomers as observed in coherent two-dimensional electronic spectroscopy.[56]

We have performed a quantum-chemical calculation of the core TBI molecule with (1,1,3,3-tetramethylbutyl) chains replaced by methyl groups at the B3LYP/6-31G(d) level (see Methods for computational details). The resulting infrared spectrum with wavenumbers and infrared intensities (related to integral absorption coefficients) is plotted in Figure 3e. As the frequency resolution of our experimental power spectrum is low and the number of scaffold vibrations in this wavenumber range is large, we cannot precisely identify which of the vibrations contribute to the oscillating signal we observe. The peaks at wavenumbers 506 and 552 cm^{-1} are the most prominent candidates for the oscillating component at 497 cm^{-1} in the trace of Figure 3c, and their associated nuclear motions are shown in Figure 3f. In total, we attribute the full dynamics of our F-PP signal to a vibronic coherence and excited-state vibrational relaxation on a timescale of 925 fs followed by slow excited-state decay which lies outside of our measurement time window.

Having analyzed the TBI ensemble as a reference, we turn our attention to single molecules. The only change in sample preparation was to heavily dilute the stock solution used for spin coating. As a result, the density of molecules on the surface was strongly decreased, enabling imaging of individual molecules by the diffraction-limited laser focus. A typical spatial image of these samples is shown in Figure 4a, where well-separated individual molecules can be seen on the surface. As we excited the molecules with linearly polarized light, the variation in brightness

between molecules stems mainly from the overlap in laser polarization and the molecular transition dipole moment, which depends on the molecule's orientation on the surface.

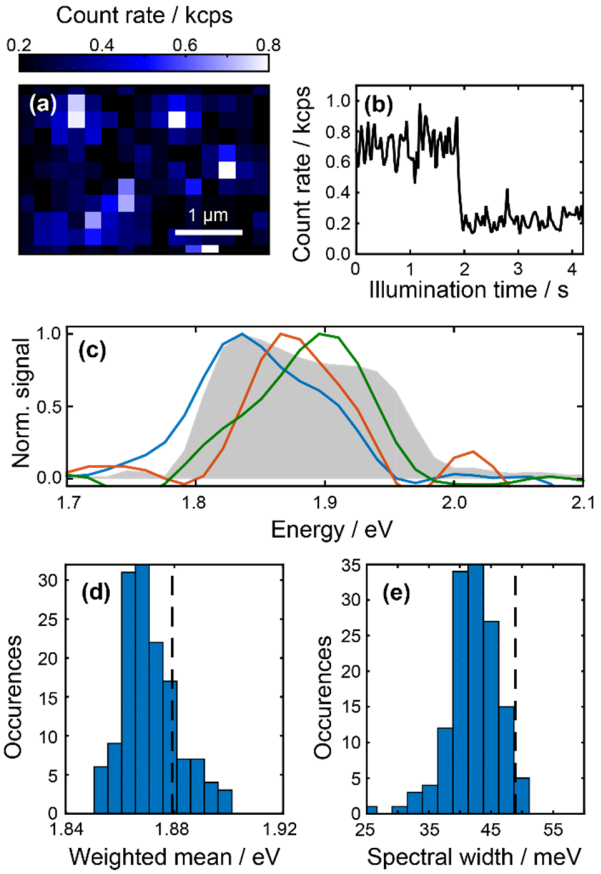

Figure 4. Single-molecule static micro-spectroscopy of TBI. (a) Spatial fluorescence image of a heavily diluted TBI sample, showing well-separated single molecules. (b) Single-step photobleaching of an individual molecule under constant illumination by the femtosecond pump laser. (c) Exemplary single-molecule linear spectra (blue, green, red) in qualitative comparison with the ensemble spectrum (shaded grey). (d, e) Distributions of the weighted mean (d) and spectral width as obtained from the second moment (e) of the single-molecule linear spectra (blue histograms) in comparison to the ensemble sample (dashed lines).

Besides our microscope images displaying clearly separated features, the individual objects demonstrated the typical blinking and single-step photobleaching behavior that is expected of single molecules, with an exemplary time trace displayed in Figure 4b. Overall, the observed TBI

molecules exhibited, at our excitation intensities, a broad range of survival times from several seconds to half an hour before eventual irreversible photobleaching, which is in agreement with single-molecule experiments on other rylene dyes in polymer matrices.[57] While the molecules exhibited single-step photobleaching behavior, only few blinking events and almost no spectral diffusion were seen in most TBI molecules.

To ensure that the spots observed in Figure 4a indeed result from single TBI molecules and not from fluorescent contaminants, we performed a reference measurement on a spin-coated sample containing only PMMA. As a result, we observed no hot spots at all in our fluorescence images, thus excluding contamination from PMMA, the solvents or the glass substrate. We further performed extensive characterization of the TBI compound used for spin-coating (Supporting Information, Section S5) and an F-PP measurement without sample to rule out measurement artifacts originating from nonlinear behavior of the photon counter (Supporting Information, Section S6). We therefore conclude that the observed hot-spot signals in the microscope images indeed result only from individual TBI molecules.

Some examples of the linear spectra obtained of individual molecules are illustrated along with the ensemble measurement in Figure 4c. The peak position of these examples strongly varies, and all three are much narrower than the ensemble reference. To quantify this observation, we performed the measurement on a total of 138 single molecules and calculated the first and second moment for each linear spectrum, corresponding to the weighted mean and the variance around this mean, respectively. These two quantities give information about the spectral positions and widths of the individual molecules, and the results are shown as histograms in Figures 4d and 4e, respectively, with the same evaluation performed for the ensemble measurement for reference (dashed vertical lines).

The weighted mean for individual molecules is distributed around a mean value of 1.87 eV, which differs only slightly from the ensemble with a mean value of 1.88 eV. In general, these two values should be identical if the single molecules were randomly picked, thus being representative of the ensemble measurement. However, there is a bias in the single-molecule data because in our experiments, only the brightest molecules were chosen to get the highest signal for the nonlinear spectra. For our given measurement parameters, molecules with a red-shifted resonance will show the highest total efficiency in excitation and detection (because of the choice of excitation wavelength and detection spectral cut-off), leading to the highest photon counts in our microscope images (Supporting Information, Section S7). This explains the slight observed red shift in the histogram of Figure 4d. For the second moment, it is seen that almost all single-molecule spectra exhibit a smaller linewidth than the reference. This is in general expected because the ensemble spectrum emerges from the average of many molecules, each with a slightly different resonance and individual smaller linewidth, ultimately leading to a smeared-out spectrum due to inhomogeneous broadening. Since we observe the second moments to be on the same scale as the distribution of first moments, we were not able to resolve any spectral diffusion for most TBI molecules.

The linear spectrum is obtained for every T step of an F-PP measurement, and thus one might expect that there should be an equivalent number of nonlinear spectra for the single molecules. This is, however, not fulfilled because the number of waiting time steps that can be measured on a single molecule can vary strongly from molecule to molecule due to the unpredictability of the permanent photobleaching event after which no fluorescence is detected anymore and the data acquisition has to be stopped. For some molecules this leads to a very small number of accessible waiting time steps, which makes any analysis of time-dependent behavior impossible. For this

reason, the initial dataset of 138 single-molecule spectra was filtered, and we took into account only those molecules that survived at least seven *T* steps, corresponding to a maximum time delay of 250 fs. The resulting spectra are much noisier than the linear spectra because the nonlinear F-PP signal is a difference measurement by nature. Therefore, the dataset was filtered further, keeping only those spectra with a signal-to-noise ratio >1 when summed over the waiting time *T* (by comparing the signal region to another spectral region, containing noise only, of equal size), such that a total of 24 single-molecule F-PP spectra remained.

An example F-PP spectrum of a single molecule with full time-delay range up to 1.5 ps is shown in Figure 5a. Like in the ensemble reference F-PP spectrum in Figure 3a, the signal is negative. In the time-integrated spectrum (Figure 5b), the main peak from the molecule is clearly visible despite more noise.

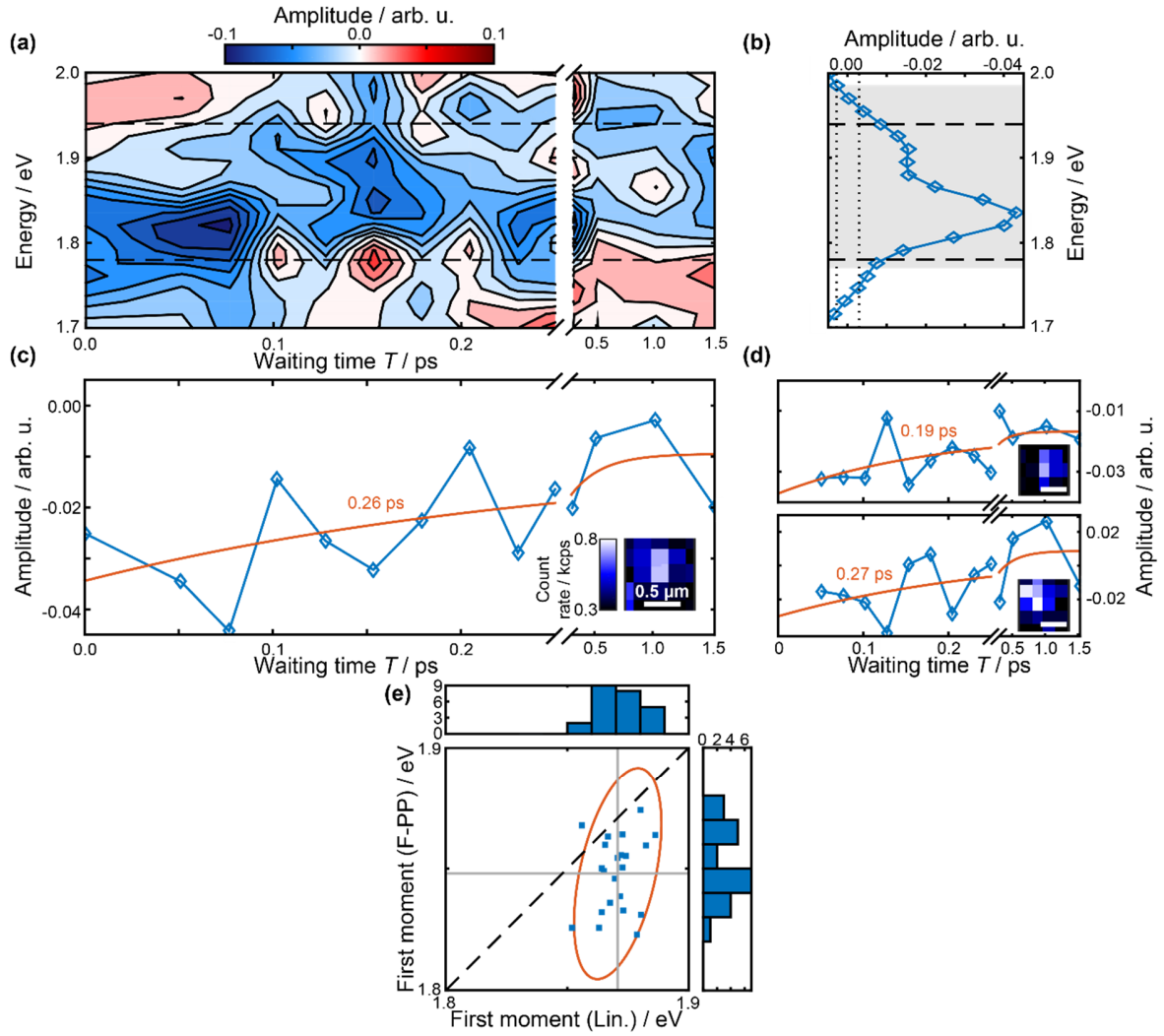

Figure 5. Single-molecule F-PP micro-spectroscopy of TBI. (a) Time-resolved F-PP spectrum of an individual molecule with linear sampling up to 0.25 ps and subsequent nonlinear sampling. Spectral integration limits for the time trace are indicated with dashed lines. (b) F-PP spectrum integrated over *T*. The grey-shaded area indicates the signal window, and the dotted lines give an estimation of the noise floor, both for positive and negative signals (Supporting Information, Section S4). (c) Spectrally integrated time trace of the F-PP signal (blue), demonstrating the negative, decaying signal and kinetic exponential fit (red) with extracted time constant. The inset depicts a fluorescence image of the single molecule. (d) Two other single-molecule F-PP transients with similar time constants. (e) Correlation of the first moments of linear and F-PP spectra of the same molecules with individual data points given as histograms. The 95% confidence interval is given in red, and the mean value of each histogram is shown with grey lines. For visualization, the diagonal is indicated with a dashed line.

We integrated the F-PP spectrum along the energy axis from 1.78 to 1.94 eV (Figure 5c) and applied the same type of kinetic fit as in Figure 3c, yielding a time constant of 0.26 ps. This corresponds to ~4 times faster dynamics in this individual molecule compared to the ensemble sample. Similar behavior is seen in two other single molecules (Figure 5d), with associated time constants of 0.19 and 0.27 ps. It is surprising that the time constants for individual molecules are smaller than for the ensemble sample. However, this behavior is found in only three F-PP transients and the other measurements were too noisy to evaluate such that we cannot make a statistical statement about the distribution of the time constants of individual molecules like we could for the linear spectra. The local environment of a single emitter can have a strong influence on decay rates associated with the system. For example, the environment might change molecular conformation leading to modified rates of both vibrational relaxation and spontaneous emission. These rates are in direct competition to the rate of photobleaching, which means that faster relaxation makes permanent photobleaching less likely for each excitation process. This change in molecular conformation induced by a local environment would then explain both the observed faster rate of vibrational relaxation in a single molecule compared to the ensemble and why the molecules we observed survive our measurement conditions for such a long time.

Both stimulated emission and ground-state bleach contribute to a F-PP spectrum, and hence we can use the method to learn something about the transition frequencies between vibronic states of a single molecule. For this, we calculated the first moment of all 24 F-PP spectra averaged along T (see Supporting Information S8 for the full spectra) and show the result along with the correlation of the first moments of linear and F-PP spectra of the same respective molecules in Figure 5e. On average, the weighted mean of the F-PP spectrum is red-shifted in comparison to the linear spectrum. This can be intuitively understood: While a ground-state bleach gives the same

information as the linear spectrum, the F-PP spectrum includes stimulated emission in addition, which is red-shifted with respect to the ground-state bleach and includes lower-energy transitions (see Supporting Information S9 for a more detailed explanation).

The correlation of the linear and nonlinear spectra provides insight into the sensitivity of the excited state to the molecular environment. In general, the ground- and excited-state potentials are displaced from each other. The vertical distance determines the transition frequency, and its environment-induced fluctuations affect the weighted mean of absorption and stimulated emission spectra in the same way.[57] In contrast, the horizontal displacement along a generalized vibrational coordinate changes the Franck–Condon factors of individual transitions while the transition frequencies remain constant. As long as the mirror-image rule between absorption and emission spectrum holds, this change in spectral shape will shift the weighted mean of absorption and emission spectrum in opposite directions.[58] Since our spectra were measured at room temperature, the resulting spectral features are broad and we assume that this mirror image approximation is valid in our case. Consequently, the first moments of the linear and F-PP spectra should in our case be directly correlated, as in either case, absorption and ground-state bleach are shifted in tandem.

The linear correlation coefficient between the first moments of linear and F-PP spectra, each evaluated for the same single molecule, is 0.46 (p = 0.02). The main contributing factor to the variation in transition frequencies and the resulting correlation of linear/nonlinear spectral positions is most probably an environment-induced change in molecular conformation from molecule to molecule.

In summary, we have introduced F-PP micro-spectroscopy and verified the technique on an ensemble of highly stable TBI molecules in PMMA matrix. We observed wave-packet dynamics and vibrational relaxation on a femtosecond timescale. We then investigated single molecules and showed that our technique is sensitive to environment-induced changes in both spectral width as well as position. Finally, we have measured single-molecule F-PP spectra for a total of 24 individual molecules, where we have seen heterogeneous behavior in both the spectral positions and the ultrafast intramolecular relaxation processes. We have analyzed the impact of the local matrix environment on the transition frequencies between vibronic states.

The method has advantages compared to other ultrafast single-molecule approaches because it has a simple beam geometry, is a direct analogue of coherently detected transient absorption, and thus benefits from a large body of past literature and established interpretation techniques, such as global analysis.[50,59] The only mandatory parameters to change for the experiment are the time delays, which can be adjusted in a multitude of ways such as using interferometers as we have done here, but also with pulse shapers or wedge pairs[60,61], making the method compatible with many setups. The approach can be further extended by, e.g., shot-to-shot detection[62], phase cycling[63], time-correlated single photon counting, or photon correlation measurements.

With its broad applicability and the mentioned benefits of F-PP microscopy, the approach presented here makes it possible to overcome previous experimental obstacles to the investigation of ultrafast phenomena in single quantum systems.

METHODS.

Time-resolved spectroscopy. We used a commercial Yb-doped fiber laser (Amplitude Systèmes, Tangerine HP) to pump a noncollinear optical parametric amplifier of our own design,[64] yielding pulses in the visible (center wavelength of 661 nm) at 1012.5 kHz repetition rate. This output was compressed using a prism compressor and a liquid-crystal-display-based pulse shaper (Jenoptik, SLM-S640d USB). We used a commercial autocorrelator (APE GmbH, pulseCheck) and second-harmonic-generation frequency-resolved optical gating for pulse characterization. Pulses were split into an identical pair using thin glass wedges (Hellma Optics, Fused Silica wedges, 1 mm thick edge, 60 arcmin, uncoated), with the reflection serving as the pump pulse. The transmission was split further into a probe pulse pair using a Mach–Zehnder interferometer, yielding a total of three compressed pulses after recombination by another wedge pair, with time delays that were individually adjustable by piezo stages (Newport Corporation, NPX400SG). To remove the coherence between pump and probe pair, the delay stage used to adjust the waiting time T was wobbled slightly using a vibrational motor. This pulse train was then guided into a laser-scanning microscope of our own design and focused by a Schwarzschild objective (Beck Optronic Solutions, 5006-000, NA = 0.65) to excite a diffraction-limited spot on a sample. Sample fluorescence was collected by a refractive objective (Carl Zeiss AG, Achroplan, NA = 0.80) and separated from remaining excitation light by three identical, successive long-pass filters (Thorlabs, Inc., FELH0700). Confocal detection was enabled by guiding fluorescence light through a single-mode fiber (Thorlabs, Inc., SM600) before detection by a single-photon counting module (Excelitas Technologies Corp., SPCM-AQRH-14-FC). To generate images, the sample was scanned laterally using a triaxial piezo inertia drive stage (Mechonics MS30/PS30). Data was acquired and evaluated using custom-built programs and scripts in LabView 2014 and MATLAB R2015a. A demonstration of the spatial and temporal resolution can be found in Supporting

Information, Sections S1 and S2, respectively. Before Fourier transformation, interferograms were zero-padded to three times their length to increase number of points in the frequency domain. Last, F-PP spectra were scaled by a constant factor determined by the area of the linear spectrum. This spectral area is related to the total photocounts in the measurement, and the resulting amplitude of the F-PP spectrum after scaling gives a measure of the ratio of nonlinear to linear signal, thus making amplitudes comparable between measurements without affecting the transient behavior or spectral positions.

Sample preparation. For all measurements, a stock solution of TBI in toluene (Merck KGaA, Toluene for spectroscopy Uvasol®) with an optical density of 0.022 was prepared. Solutions for spin coating were prepared daily by diluting the stock solution with a 50/50 mixture of toluene and PMMA in solution (Allresist GmbH, AR-P 671.02 950K) to final concentrations of 2.19 µmol/l and 0.27 nmol/l (or dilution factors of 5 and 40000) for the ensemble and single-molecule samples, respectively. 10 µL of these diluted solutions were finally spin-coated onto cleaned cover glasses at 2000 rpm.

Steady-state absorption and fluorescence. The steady-state absorption and emission spectra were measured with a Jasco V-670 spectrophotometer and an Edinburgh Instruments FLS980 spectrometer (excitation wavelength at 620 nm), respectively.

Quantum-chemical simulations. The quantum-chemical calculation of the TBI molecule with (1,1,3,3-tetramethylbutyl) chains replaced by methyl groups was performed using Gaussian 09[65] at the B3LYP/6-31G(d) level with the *opt* and *freq* keywords, corresponding to geometry optimization and calculation of molecular vibrations. The approximation of the 1,1,3,3-tetramethylbutyl moieties as simple methyl groups is justified due to the high computational cost

associated with the long alkyl chains, with their main function being sterical hindrance between molecules, which is not considered in the calculation. The TBI scaffold, which gives rise to the electronic properties of the dye, is fully present in this calculation. After calculation, an empirical scaling factor for the DFT method (0.962) was applied to the calculated frequencies.[66]

ASSOCIATED CONTENT

Supporting Information.

The following file is available free of charge.

Spatial resolution, Pulse characterization at the sample position, Morphology of the ensemble sample, Estimation of the noise floor of F-PP spectra, Synthesis and characterization of TBI, F-PP measurement without sample, Explanation of red shift seen in the linear spectra of single molecules, Mean linear and F-PP spectra used for statistical analysis, and Systematic red shift in the first moments of linear and F-PP spectra (PDF)

AUTHOR INFORMATION

Corresponding Author

Tobias Brixner

Notes

The authors declare no competing financial interests.

ACKNOWLEDGMENTS

We thank Jürgen Köhler (Bayreuth) for practical advice on single-molecule spectroscopy and Thomas Basché (Mainz) for pointing out the stability of terrylene dyes. TB acknowledges funding

by the Deutsche Forschungsgemeinschaft (DFG, German Research Foundation) – 410519108. PM acknowledges support by the Alexander von Humboldt foundation and funding from the European Union's Horizon 2020 research and innovation program under the Marie Skłodowska-Curie grant agreement No 101030656.

REFERENCES

(1) Moerner, W. E. A Dozen Years of Single-Molecule Spectroscopy in Physics, Chemistry, and Biophysics. *J. Phys. Chem. B* **2002**, *106*, 910–927.
(2) Orrit, M.; Bernard, J. Single Pentacene Molecules Detected by Fluorescence Excitation in a P-Terphenyl Crystal. *Phys. Rev. Lett.* **1990**, *65*, 2716–2719.
(3) Moerner, W. E. Examining Nanoenvironments in Solids on the Scale of a Single, Isolated Impurity Molecule. *Science* **1994**, *265*, 46–53.
(4) Moerner, W. E.; Basché, T. Optical Spectroscopy of Single Impurity Molecules in Solids. *Angew. Chem. Int. Ed. Engl.* **1993**, *32*, 457–476.
(5) Kador, L.; Horne, D. E.; Moerner, W. E. Optical Detection and Probing of Single Dopant Molecules of Pentacene in a P-Terphenyl Host Crystal by Means of Absorption Spectroscopy. *J. Phys. Chem.* **1990**, *94*, 1237–1248.
(6) Basché, Th.; Moerner, W. E.; Orrit, M.; Talon, H. Photon Antibunching in the Fluorescence of a Single Dye Molecule Trapped in a Solid. *Phys. Rev. Lett.* **1992**, *69*, 1516–1519.
(7) Toninelli, C.; Gerhardt, I.; Clark, A. S.; Reserbat-Plantey, A.; Götzinger, S.; Ristanović, Z.; Colautti, M.; Lombardi, P.; Major, K. D.; Deperasińska, I.; Pernice, W. H.; Koppens, F. H. L.; Kozankiewicz, B.; Gourdon, A.; Sandoghdar, V.; Orrit, M. Single Organic Molecules for Photonic Quantum Technologies. *Nat. Mater.* **2021**, *20*, 1615–1628.
(8) Lelek, M.; Gyparaki, M. T.; Beliu, G.; Schueder, F.; Griffié, J.; Manley, S.; Jungmann, R.; Sauer, M.; Lakadamyali, M.; Zimmer, C. Single-Molecule Localization Microscopy. *Nat. Rev. Methods Primer* **2021**, *1*, 39.
(9) Schermelleh, L.; Ferrand, A.; Huser, T.; Eggeling, C.; Sauer, M.; Biehlmaier, O.; Drummen, G. P. C. Super-Resolution Microscopy Demystified. *Nat. Cell Biol.* **2019**, *21*, 72–84.
(10) Rust, M. J.; Bates, M.; Zhuang, X. Sub-Diffraction-Limit Imaging by Stochastic Optical Reconstruction Microscopy (STORM). *Nat. Methods* **2006**, *3*, 793–796.
(11) Sauer, M. Localization Microscopy Coming of Age: From Concepts to Biological Impact. *J. Cell Sci.* **2013**, *126*, 3505–3513.
(12) Betzig, E. Proposed Method for Molecular Optical Imaging. *Opt. Lett.* **1995**, *20*, 237–239.
(13) van Oijen, A. M.; Köhler, J.; Schmidt, J.; Müller, M.; Brakenhoff, G. J. 3-Dimensional Super-Resolution by Spectrally Selective Imaging. *Chem. Phys. Lett.* **1998**, *292*, 183–187.
(14) Betzig, E.; Patterson, G. H.; Sougrat, R.; Lindwasser, O. W.; Olenych, S.; Bonifacino, J. S.; Davidson, M. W.; Lippincott-Schwartz, J.; Hess, H. F. Imaging Intracellular Fluorescent Proteins at Nanometer Resolution. *Science* **2006**, *313*, 1642–1645.
(15) Bates, M.; Huang, B.; Dempsey, G. T.; Zhuang, X. Multicolor Super-Resolution Imaging with Photo-Switchable Fluorescent Probes. *Science* **2007**, *317*, 1749–1753.

(16) Weston, K. D.; Carson, P. J.; Metiu, H.; Buratto, S. K. Room-Temperature Fluorescence Characteristics of Single Dye Molecules Adsorbed on a Glass Surface. *J. Chem. Phys.* **1998**, *109*, 7474–7485.
(17) Novotny, L.; van Hulst, N. Antennas for Light. *Nat. Photonics* **2011**, *5*, 83–90.
(18) Anger, P.; Bharadwaj, P.; Novotny, L. Enhancement and Quenching of Single-Molecule Fluorescence. *Phys. Rev. Lett.* **2006**, *96*, 113002.
(19) Kühn, S.; Håkanson, U.; Rogobete, L.; Sandoghdar, V. Enhancement of Single-Molecule Fluorescence Using a Gold Nanoparticle as an Optical Nanoantenna. *Phys. Rev. Lett.* **2006**, *97*, 017402.
(20) Kinkhabwala, A.; Yu, Z.; Fan, S.; Avlasevich, Y.; Müllen, K.; Moerner, W. E. Large Single-Molecule Fluorescence Enhancements Produced by a Bowtie Nanoantenna. *Nat. Photonics* **2009**, *3*, 654–657.
(21) Chikkaraddy, R.; de Nijs, B.; Benz, F.; Barrow, S. J.; Scherman, O. A.; Rosta, E.; Demetriadou, A.; Fox, P.; Hess, O.; Baumberg, J. J. Single-Molecule Strong Coupling at Room Temperature in Plasmonic Nanocavities. *Nature* **2016**, *535*, 127–130.
(22) Schörner, C.; Lippitz, M. Single Molecule Nonlinearity in a Plasmonic Waveguide. *Nano Lett.* **2020**, *20*, 2152–2156.
(23) Zürner, A.; Kirstein, J.; Döblinger, M.; Bräuchle, C.; Bein, T. Visualizing Single-Molecule Diffusion in Mesoporous Materials. *Nature* **2007**, *450*, 705–708.
(24) Baier, M.; Wöll, D.; Mecking, S. Diffusion of Molecular and Macromolecular Polyolefin Probes in Cylindrical Block Copolymer Structures as Observed by High Temperature Single Molecule Fluorescence Microscopy. *Macromolecules* **2018**, *51*, 1873–1884.
(25) Wöll, D.; Uji-i, H.; Schnitzler, T.; Hotta, J.; Dedecker, P.; Herrmann, A.; De Schryver, F. C.; Müllen, K.; Hofkens, J. Radical Polymerization Tracked by Single Molecule Spectroscopy. *Angew. Chem. Int. Ed.* **2008**, *47*, 783–787.
(26) Erker, C.; Basché, T. The Energy Gap Law at Work: Emission Yield and Rate Fluctuations of Single NIR Emitters. *J. Am. Chem. Soc.* **2022**, *144*, 14053–14056.
(27) Wilma, K.; Issac, A.; Chen, Z.; Würthner, F.; Hildner, R.; Köhler, J. Tracing Single Electrons in a Disordered Polymer Film at Room Temperature. *J. Phys. Chem. Lett.* **2016**, *7*, 1478–1483.
(28) Hou, S.; Exell, J.; Welsher, K. Real-Time 3D Single Molecule Tracking. *Nat. Commun.* **2020**, *11*, 3607.
(29) Stracy, M.; Uphoff, S.; Garza de Leon, F.; Kapanidis, A. N. In Vivo Single-Molecule Imaging of Bacterial DNA Replication, Transcription, and Repair. *FEBS Lett.* **2014**, *588*, 3585–3594.
(30) Sasmal, D. K.; Pulido, L. E.; Kasal, S.; Huang, J. Single-Molecule Fluorescence Resonance Energy Transfer in Molecular Biology. *Nanoscale* **2016**, *8*, 19928–19944.
(31) Jungmann, R.; Steinhauer, C.; Scheible, M.; Kuzyk, A.; Tinnefeld, P.; Simmel, F. C. Single-Molecule Kinetics and Super-Resolution Microscopy by Fluorescence Imaging of Transient Binding on DNA Origami. *Nano Lett.* **2010**, *10*, 4756–4761.
(32) Berera, R.; Grondelle, R. van; Kennis, J. T. M. Ultrafast Transient Absorption Spectroscopy: Principles and Application to Photosynthetic Systems. *Photosynth. Res.* **2009**, *101*, 105–118.
(33) Kukura, P.; Celebrano, M.; Renn, A.; Sandoghdar, V. Single-Molecule Sensitivity in Optical Absorption at Room Temperature. *J. Phys. Chem. Lett.* **2010**, *1*, 3323–3327.
(34) Maser, A.; Gmeiner, B.; Utikal, T.; Götzinger, S.; Sandoghdar, V. Few-Photon Coherent Nonlinear Optics with a Single Molecule. *Nat. Photonics* **2016**, *10*, 450–453.

(35) Moerner, W. E. Single-Molecule Spectroscopy, Imaging, and Photocontrol: Foundations for Super-Resolution Microscopy (Nobel Lecture). *Angew. Chem. Int. Ed.* **2015**, *54*, 8067–8093.
(36) Guenther, T.; Lienau, C.; Elsaesser, T.; Glanemann, M.; Axt, V.; Kuhn, T.; Eshlaghi, S.; Wieck, A. Coherent Nonlinear Optical Response of Single Quantum Dots Studied by Ultrafast Near-Field Spectroscopy. *Phys. Rev. Lett.* **2002**, *89*, 057401.
(37) Langbein, W.; Patton, B. Transient Coherent Nonlinear Spectroscopy of Single Quantum Dots. *J. Phys. Condens. Matter* **2007**, *19*, 295203.
(38) Mermillod, Q.; Wigger, D.; Delmonte, V.; Reiter, D. E.; Schneider, C.; Kamp, M.; Höfling, S.; Langbein, W.; Kuhn, T.; Nogues, G.; Kasprzak, J. Dynamics of Excitons in Individual InAs Quantum Dots Revealed in Four-Wave Mixing Spectroscopy. *Optica* **2016**, *3*, 377–384.
(39) Piatkowski, L.; Accanto, N.; Calbris, G.; Christodoulou, S.; Moreels, I.; van Hulst, N. F. Ultrafast Stimulated Emission Microscopy of Single Nanocrystals. *Science* **2019**, *366*, 1240–1243.
(40) Birkmeier, K.; Hertel, T.; Hartschuh, A. Probing the Ultrafast Dynamics of Excitons in Single Semiconducting Carbon Nanotubes. *Nat. Commun.* **2022**, *13*, 6290.
(41) Cocker, T. L.; Peller, D.; Yu, P.; Repp, J.; Huber, R. Tracking the Ultrafast Motion of a Single Molecule by Femtosecond Orbital Imaging. *Nature* **2016**, *539*, 263–267.
(42) Schedlbauer, J.; Wilhelm, P.; Grabenhorst, L.; Federl, M. E.; Lalkens, B.; Hinderer, F.; Scherf, U.; Höger, S.; Tinnefeld, P.; Bange, S.; Vogelsang, J.; Lupton, J. M. Ultrafast Single-Molecule Fluorescence Measured by Femtosecond Double-Pulse Excitation Photon Antibunching. *Nano Lett.* **2020**, *20*, 1074–1079.
(43) Moya, R.; Kondo, T.; Norris, A. C.; Schlau-Cohen, G. S. Spectrally-Tunable Femtosecond Single-Molecule Pump-Probe Spectroscopy. *Opt. Express* **2021**, *29*, 28246.
(44) Moya, R.; Norris, A. C.; Kondo, T.; Schlau-Cohen, G. S. Observation of Robust Energy Transfer in the Photosynthetic Protein Allophycocyanin Using Single-Molecule Pump–Probe Spectroscopy. *Nat. Chem.* **2022**, *14*, 153–159.
(45) Malý, P.; Gruber, J. M.; Cogdell, R. J.; Mančal, T.; van Grondelle, R. Ultrafast Energy Relaxation in Single Light-Harvesting Complexes. *Proc. Natl. Acad. Sci.* **2016**, *113*, 2934–2939.
(46) Hildner, R.; Brinks, D.; Nieder, J. B.; Cogdell, R. J.; Hulst, N. F. van. Quantum Coherent Energy Transfer over Varying Pathways in Single Light-Harvesting Complexes. *Science* **2013**, *340*, 1448–1451.
(47) Brinks, D.; Hildner, R.; Dijk, E. M. H. P. van; Stefani, F. D.; Nieder, J. B.; Hernando, J.; Hulst, N. F. van. Ultrafast Dynamics of Single Molecules. *Chem. Soc. Rev.* **2014**, *43*, 2476–2491.
(48) Hildner, R.; Brinks, D.; Hulst, N. F. van. Femtosecond Coherence and Quantum Control of Single Molecules at Room Temperature. *Nat. Phys.* **2011**, *7*, 172–177.
(49) Liebel, M.; Toninelli, C.; van Hulst, N. F. Room-Temperature Ultrafast Nonlinear Spectroscopy of a Single Molecule. *Nat. Photonics* **2018**, *12*, 45–49.
(50) Malý, P.; Brixner, T. Fluorescence-Detected Pump–Probe Spectroscopy. *Angew. Chem. Int. Ed.* **2021**, *60*, 18867–18875.
(51) Piatkowski, L.; Gellings, E.; van Hulst, N. F. Broadband Single-Molecule Excitation Spectroscopy. *Nat. Commun.* **2016**, *7*, 10411.
(52) Perri, A.; Preda, F.; D'Andrea, C.; Thyrhaug, E.; Cerullo, G.; Polli, D.; Hauer, J. Excitation-Emission Fourier-Transform Spectroscopy Based on a Birefringent Interferometer. *Opt. Express* **2017**, *25*, A483–A490.

(53) Nolde, F.; Qu, J.; Kohl, C.; Pschirer, N. G.; Reuther, E.; Müllen, K. Synthesis and Modification of Terrylenediimides as High-Performance Fluorescent Dyes. *Chem. – Eur. J.* **2005**, *11*, 3959–3967.
(54) Weil, T.; Vosch, T.; Hofkens, J.; Peneva, K.; Müllen, K. The Rylene Colorant Family-Tailored Nanoemitters for Photonics Research and Applications. *Angew. Chem. Int. Ed.* **2010**, *49*, 9068–9093.
(55) Braeken, E.; De Cremer, G.; Marsal, P.; Pèpe, G.; Müllen, K.; Vallée, R. A. L. Single Molecule Probing of the Local Segmental Relaxation Dynamics in Polymer above the Glass Transition Temperature. *J. Am. Chem. Soc.* **2009**, *131*, 12201–12210.
(56) Schultz, J. D.; Shin, J. Y.; Chen, M.; O'Connor, J. P.; Young, R. M.; Ratner, M. A.; Wasielewski, M. R. Influence of Vibronic Coupling on Ultrafast Singlet Fission in a Linear Terrylenediimide Dimer. *J. Am. Chem. Soc.* **2021**, *143*, 2049–2058.
(57) Streiter, M.; Krause, S.; von Borczyskowski, C.; Deibel, C. Dynamics of Single-Molecule Stokes Shifts: Influence of Conformation and Environment. *J. Phys. Chem. Lett.* **2016**, *7*, 4281–4284.
(58) de Jong, M.; Seijo, L.; Meijerink, A.; Rabouw, F. T. Resolving the Ambiguity in the Relation between Stokes Shift and Huang–Rhys Parameter. *Phys. Chem. Chem. Phys.* **2015**, *17*, 16959–16969.
(59) van Stokkum, I. H. M.; Larsen, D. S.; van Grondelle, R. Global and Target Analysis of Time-Resolved Spectra. *Biochim. Biophys. Acta BBA - Bioenerg.* **2004**, *1657*, 82–104.
(60) Brixner, T.; Stiopkin, I. V.; Fleming, G. R. Tunable Two-Dimensional Femtosecond Spectroscopy. *Opt. Lett.* **2004**, *29*, 884–886.
(61) Brida, D.; Manzoni, C.; Cerullo, G. Phase-Locked Pulses for Two-Dimensional Spectroscopy by a Birefringent Delay Line. *Opt. Lett.* **2012**, *37*, 3027–3029.
(62) Kanal, F.; Keiber, S.; Eck, R.; Brixner, T. 100-KHz Shot-to-Shot Broadband Data Acquisition for High-Repetition-Rate Pump–Probe Spectroscopy. *Opt. Express* **2014**, *22*, 16965–16975.
(63) Tan, H.-S. Theory and Phase-Cycling Scheme Selection Principles of Collinear Phase Coherent Multi-Dimensional Optical Spectroscopy. *J. Chem. Phys.* **2008**, *129*, 124501.
(64) Huber, B.; Pres, S.; Wittmann, E.; Dietrich, L.; Lüttig, J.; Fersch, D.; Krauss, E.; Friedrich, D.; Kern, J.; Lisinetskii, V.; Hensen, M.; Hecht, B.; Bratschitsch, R.; Riedle, E.; Brixner, T. Space- and Time-Resolved UV-to-NIR Surface Spectroscopy and 2D Nanoscopy at 1 MHz Repetition Rate. *Rev. Sci. Instrum.* **2019**, *90*, 113103.
(65) Frisch, M. J.; Trucks, G. W.; Schlegel, H. B.; Scuseria, G. E.; Robb, M. A.; Cheeseman, J. R.; Scalmani, G.; Barone, V.; Mennucci, B.; Petersson, G. A.; Nakatsuji, H.; Caricato, M.; Li, X.; Hratchian, H. P.; Izmaylov, A. F.; Bloino, J.; Zheng, G.; Sonnenberg, J. L.; Hada, M.; Ehara, M.; Toyota, K.; Fukuda, R.; Hasegawa, J.; Ishida, M.; Nakajima, T.; Honda, Y.; Kitao, O.; Nakai, H.; Vreven, T.; Montgomery, Jr., J. A.; Peralta, J. E.; Ogliaro, F.; Bearpark, M.; Heyd, J. J.; Brothers, E.; Kudin, K. N.; Staroverov, V. N.; Kobayashi, R.; Normand, J.; Raghavachari, K.; Rendell, A.; Burant, J. C.; Iyengar, S. S.; Tomasi, J.; Cossi, M.; Rega, N.; Millam, J. M.; Klene, M.; Knox, J. E.; Cross, J. B.; Bakken, V.; Adamo, C.; Jaramillo, J.; Gomperts, R.; Stratmann, R. E.; Yazyev, O.; Austin, A. J.; Cammi, R.; Pomelli, C.; Ochterski, J. W.; Martin, R. L.; Morokuma, K.; Zakrzewski, V. G.; Voth, G. A.; Salvador, P.; Dannenberg, J. J.; Dapprich, S.; Daniels, A. D.; Farkas, Ö.; Foresman, J. B.; Ortiz, J. V.; Cioslowski, J.; Fox, D. J. *Gaussian 09, Revision D.01*; Gaussian, Inc.: Wallingford CT, 2013.

(66) Johnson, R. *Computational Chemistry Comparison and Benchmark Database*. NIST Standard Reference Database Number 101. http://cccbdb.nist.gov/ (accessed 2022-12-08).